JACC: CLINICAL ELECTROPHYSIOLOGY VOL. 8, NO. 2, 2022

PUBLISHED BY ELSEVIER

CIED - IMAGING

Detailed Assessment of Low-Voltage Zones Localization by Cardiac MRI in Patients With Implantable Devices

Michele Orini, PhD,[a,b,*] Andreas Seraphim, MBBS,[a,b,*] Adam Graham, PhD,[b] Anish Bhuva, PhD,[a,c] Ernesto Zacur, PhD,[d] Peter Kellman, PhD,[e] Richard Schilling, MD,[b] Ross Hunter, PhD,[b] Mehul Dhinoja, MD,[b] Malcolm C. Finlay, PhD,[b] Syed Ahsan, MD,[b] Anthony W. Chow, MD,[b] James C. Moon, MD,[a,c] Pier D. Lambiase, PhD,[a,b,†] Charlotte Manisty, PhD[a,c,†]

ABSTRACT

OBJECTIVES The purpose of this study was to assess the performance and limitations of low-voltage zones (LVZ) localization by optimized late gadolinium enhancement (LGE) cardiac magnetic resonance (CMR) scar imaging in patients with cardiac implantable electronic devices (CIEDs).

BACKGROUND Scar evaluation by LGE-CMR can assist ventricular tachycardia (VT) ablation, but challenges with electroanatomical maps coregistration and presence of imaging artefacts from CIED limit accuracy.

METHODS A total of 10 patients underwent VT ablation and preprocedural LGE-CMR using wideband imaging. Scar was segmented from CMR pixel signal intensity maps using commercial software (ADAS-VT, Galgo Medical) with bespoke tools and compared with detailed electroanatomical maps (CARTO). Coregistration of EP and imaging-derived scar was performed using the aorta as a fiducial marker, and the impact of coregistration was determined by assessing intraobserver/interobserver variability and using computer simulations. Spatial smoothing was applied to assess correlation at different spatial resolutions and to reduce noise.

RESULTS Pixel signal intensity maps localized low-voltage zones (V <1.5 mV) with area under the receiver-operating characteristic curve: 0.82 (interquartile range [IQR]: 0.76-0.83), sensitivity 74% (IQR: 71%-77%), and specificity 78% (IQR: 73%-83%) and correlated with bipolar voltage (r = −0.57 [IQR: −0.68 to −0.42]) across patients. In simulations, small random shifts and rotations worsened LVZ localization in at least some cases. The use of the full aortic geometry ensured high reproducibility of LVZ localization (r >0.86 for area under the receiver-operating characteristic curve). Spatial smoothing improved localization of LVZ. Results for LVZ with V <0.5 mV were similar.

CONCLUSIONS In patients with CIEDs, novel wideband CMR sequences and personalized coregistration strategies can localize LVZ with good accuracy and may assist VT ablation procedures. (J Am Coll Cardiol EP 2022;8:225–235) © 2022 by the American College of Cardiology Foundation.

From the [a]Institute of Cardiovascular Science, University College London, London, United Kingdom; [b]Department of Cardiac Electrophysiology, Barts Heart Centre, Barts Health NHS Trust, London, United Kingdom; [c]Department of Cardiovascular Imaging, Barts Heart Centre, Barts Health NHS Trust, London, United Kingdom; [d]Department of Biomedical Engineering, University of Oxford, Oxford, United Kingdom; and the [e]National Institutes of Health, Bethesda, Maryland, USA. *Drs Orini and Seraphim contributed equally to this work and are joint first authors. †Drs Lambiase and Manisty contributed equally to this work and are joint senior authors.

The authors attest they are in compliance with human studies committees and animal welfare regulations of the authors' institutions and Food and Drug Administration guidelines, including patient consent where appropriate. For more information, visit the Author Center.

Manuscript received May 17, 2021; revised manuscript received October 5, 2021, accepted October 8, 2021.

ISSN 2405-500X/$36.00 https://doi.org/10.1016/j.jacep.2021.10.002

ABBREVIATIONS AND ACRONYMS

CIED = cardiac implantable electronic device

EAM = electroanatomical mapping

IQR = interquartile range

LGE-CMR = late gadolinium-enhanced cardiac magnetic resonance

LVZ = low-voltage zone

PSI = pixel signal intensity

VT = ventricular tachycardia

Catheter ablation improves outcomes in patients with frequent life-threatening ventricular tachycardia (VT). However, VT recurrence rates remain unacceptably high, necessitating the pursuit of more effective ablation strategies (1). Late gadolinium enhancement cardiac magnetic resonance (LGE-CMR) can provide noninvasive visualization of arrhythmogenic substrate (2-6) and its integration with electroanatomical mapping (EAM) can improve procedural outcomes (7-9). Indeed, recent work has proposed the utilization of a CMR-guided approach (9), based on EAM system and CMR-derived scar coregistration. The integration of LGE-CMR scar maps and EAM for VT ablation is, however, not widespread. There are several reasons for this. First, the precise coregistration of whole heart LGE-CMR with EAM is challenging. Second, most patients requiring VT ablation have cardiac implantable electronic devices (CIEDs) in situ. Although scanning can now be performed safely with appropriate protocols (10,11), meaning almost all patients could now have LGE-CMR, the CIED itself generates image artefact (signal dropout, hyperintensity artefact) that hinders scar delineation. Dedicated sequences incorporating a wideband inversion pulse can reduce this (10), but few studies have examined feasibility of LGE-CMR and EAM coregistration in these patients (8,12,13) and the agreement in scar localization between the 2 modalities remains undetermined. In this study, we deploy a novel wideband LGE sequence that is fast, free-breathing, and incorporates phase-sensitive inversion recovery (10). We investigate the spatial correlation between low-voltage zones from state-of-the-art EAM and 3-dimensional (3D) CMR pixel signal intensity (PSI) maps in patients with CIEDs (10) and focused on optimal approaches for coregistration that maximize clinical utility.

SEE PAGE 236

METHODS

STUDY POPULATION. The study was approved by the National Health Service Research Ethics Committee (14/LO/0360) and Health Research Authority (HRA) and was conducted in accordance with the Declaration of Helsinki. All subjects provided written, informed consent. Ten consecutive patients (1 woman; median age 75 years; interquartile range [IQR]: 70-79 years; 9 with ischemic cardiomyopathy and 1 with nonischemic dilated cardiomyopathy) with CIEDs (5 implantable cardioverter-defibrillators [ICDs], 5 cardiac resynchronization therapy with defibrillation, 50% nonmagnetic resonance conditional) undergoing catheter VT ablation between 2017 and 2019 (8 first time, 2 repeat ablations) (**Table 1**) were included in the analysis. Specifically, patients were included if they underwent LGE-CMR shortly before catheter ablation and if a detailed left ventricular (LV) substrate map and a complete aortic geometry, including ascending, arch, and descending aorta, were collected during the electrophysiological study. In all patients, catheter ablation was performed because of recurrent VTs and frequent ICD therapy. In total, 5 cases were elective and 5 were urgent cases for treatment of incessant VT or VT storm. Among the 9 patients with ischemic cardiomyopathy, myocardial infarction was more frequently seen in the anterior wall (bullseye plot of scar distribution is shown in the Supplemental Material, Supplemental Figure 1).

CMR PROTOCOL AND DATA ANALYSIS. All patients underwent LGE-CMR before their procedure. CMR studies were performed on a 1.5-T scanner (Aera, Siemens Healthineers) using a 30-channel phased array receiver coil, scanned at Normal Operating Mode (SAR limit <2 W/kg). In brief, device interrogation and reprogramming occurred immediately before and after scanning, according to international guidelines. Patients were monitored throughout using electrocardiography (ECG) and pulse oximetry waveform assessment.

An axial stack of images through the thorax was acquired for visualization of extracardiac structures, including the thoracic ascending and descending aorta, to enable coregistration with EAM data. This used a black blood Half-Fourier Acquisition Single-shot Turbo spin Echo sequence, with 5-mm slice thickness and zero gap between slices. Late gadolinium images were acquired 10-15 min after administration of 0.1 mmol/kg of Dotarem (Guerbet S.A.). The sequence used was a 2-dimensional (2D) motion-corrected (free-breathing) single-shot FLASH sequence with a 3.9-kHz (wideband) inversion pulse, with flip angle of 10°, phase-sensitive inversion recovery (10), and 24 averages to recover signal to noise. Contiguous 4-mm short-axis slices were acquired with spatial resolution of 1.9 × 1.4 mm, which was interpolated to 1.4 × 1.4 mm for display and analysis. Epicardial and endocardial borders were segmented, generating a 3D PSI map of the LV using custom software (ADAS-VT, Galgo Medical) (6-8). A total of 9 concentric surface layers from subendocardium (10% of wall thickness) to subepicardium (90% of wall thickness) were created automatically. Subsequently, PSI maps were projected over each LV layer using a trilinear interpolation and color coding to visualize PSI distribution. PSI was normalized, with global

TABLE 1 Baseline Demographics and Clinical and CMR Data of the Patient Cohort

ID	Sex (M/F)	Age (y)	Etiology	Type of Device	MR Conditional	LVEF (%)	Artefacts (% of Myocardium)	Interval CMR-Ablation (wks)	First/Redo Ablation
1	M	68	IHD	CRT-D	No	52	13.9	0.3	First
2	M	69	IHD	ICD	Yes	34	1.4	44.3	First
3	M	79	IHD	CRT-D	No	16	0.0	0.9	Redo
4	M	84	IHD	ICD	No	19	9.7	4.0	First
5	F	79	IHD	ICD	Yes	20	9.8	0.6	First
6	M	84	IHD	ICD	No	25	10.2	0.0	First
7	M	78	IHD	CRT-D	Yes	10	8.8	0.0	Redo
8	M	56	DCM	CRT-D	No	20	28.9	0.3	First
9	M	73	IHD	ICD	Yes	41	0.2	8.3	First
10	M	72	IHD	CRT-D	Yes	23	25.9	1.0	First

CMR-EP interval: time delay between cardiac magnetic resonance (CMR) and ventricular tachycardia ablation.
CRT-D = cardiac resynchronization therapy with defibrillation; DCM = dilated cardiomyopathy; ICD = implantable cardioverter-defibrillator; IHD = ischemic heart disease.

minimum and maximum across all layers set equal to 0 and 100, respectively. A tool in the same software was also used to create a 3D surface representation of the aorta from the 2D axial anatomical images and to coregister this with the LV PSI map.

EAM PROTOCOL AND DATA ANALYSIS. Procedures were performed under conscious sedation using diamorphine and midazolam or using general anesthetic. Vascular access was obtained under ultrasound guidance using Seldinger technique via the right femoral vein and/or right femoral artery. The LV was accessed retrogradely via the aorta in all cases. Transseptal puncture was additionally performed in 4 cases to gain better overall access and mapping coverage of the LV. A full geometry of the ascending, arch, and descending aorta was created for coregistration with CMR-LGE scar meshes. Collection of this geometry took <5 minutes in each case. A voltage map was created using a multipolar catheter (Pentaray, CARTO, Biosense Webster), and the ST SF Thermocool ablation catheter was also used in some cases. Most of intracardiac mapping was performed continuously with criteria for collecting data including close tissue proximity (using Tissue Proximity Indicator for Pentaray), position stability, and contact force within 2-40*g* (when using the ablation catheter). Occasionally, data collection was performed manually. EAM generated using <100 electrode points were excluded.

CARTO-generated meshes describing the spatial distribution of bipolar voltage of the LV endocardium were exported for offline analysis. Bipolar voltage <1.5 and <0.5 mV was considered indicative of scar and dense scar, respectively.

EAM-CMR COMPARISON. PSI color-coded maps were not visible to operators during the electrophysiological study to reduce potential biases and coregistration of EAM and CMR geometries was performed retrospectively (after each case) using bespoke software (Matlab, The Mathworks, Inc) (14,15) that allows the operator to move and rotate EAM and CMR geometries and inspect the alignment under any viewpoint (Video 1). Coregistration was manually performed and visually determined by an expert independent of subsequent analysis and blinded to color-coded maps of voltage and PSI (ie, solely based on anatomical information). Emphasis was placed on the simultaneous alignment of the ascending, arch, and descending aorta, and the LV apex. No other extracardiac structure was systematically utilized. After coregistration, each vertex belonging to the EAM geometry (ie, the triangular mesh produced during cardiac mapping) was paired to the closest vertex of the PSI map, provided that the Euclidean distance (D) between them was $D \leq 8$ mm.

The impact of EAM-CMR coregistration on the localization of low-voltage zones was assessed by reproducibility analysis and simulations. Intraobserver and interobserver reproducibility was assessed by repeating coregistration twice (same operator, with more than 48 hours between repetitions) and by a second expert operator, respectively. Repeated coregistrations were compared by measuring the difference between the location of the aligned geometries as shifts and rotations (Euler's rule) along and about the XYZ axes. The simulation study was carried out as follows. After coregistration, small shifts and rotations were algorithmically applied to the EAM and low-voltage zones localization reassessed. In total, the analysis was repeated 320 times per case, consistent with configurations obtained by applying simultaneous shifts and rotations of $\pm\Delta X$ mm and $\pm\Delta X^\circ$ along and around the 3 major axes ($2^6 = 64$ configurations), where $\Delta X = 2^\circ$, 4°, 6°, 8° and 10°. Video 3 shows the effect of shifts

TABLE 2 Low-Voltage Zone Localization

	Points			V <0.5 mV					V <1.5 mV				
Patient Number	EAM Mesh	Paired (%)	Corr. Coeff.	PREV (%)	AUC	THR (%)	SENS (%)	SPEC (%)	PREV (%)	AUC (%)	THR (%)	SENS (%)	SPEC (%)
1	3,871	58	−0.54	1	–	–	–	–	22	0.76	50	74	71
2	22,669	83	−0.32	22	0.58	35	64	54	55	0.70	33	68	67
3	7,947	48	−0.68	35	0.87	46	83	77	63	0.83	42	73	79
4	7,770	43	−0.69	22	0.83	50	83	72	62	0.87	41	78	83
5	6,880	65	−0.42	30	0.77	51	80	72	56	0.69	47	64	73
6	14,952	55	−0.50	49	0.80	41	72	76	76	0.81	37	71	78
7	15,583	41	−0.73	54	0.91	53	85	87	72	0.87	46	76	86
8	8,896	61	−0.61	22	0.79	49	78	69	44	0.83	44	80	76
9	2,438	88	−0.61	5	0.75	38	81	66	36	0.83	33	77	80
10	7,674	60	−0.31	80	0.69	36	77	60	96	0.79	33	75	84
Median	7,859	59	−0.57	26	0.79	46	80	72	59	0.82	41	74	78
Q1	6,880	48	−0.68	22	0.73	37	76	65	44	0.76	33	71	73
Q3	14,952	65	−0.42	49	0.84	51	83	76	72	0.83	46	77	83

AUC = area under the receiver-operating characteristic curve; EAM = electroanatomical map; MED = median; PREV = prevalence of low-voltage zones across paired points; Q1 and Q3 = first and third quartile, respectively; SENS = sensitivity; SPEC = specificity; THR = pixel signal intensity case-specific threshold.

and rotations of up to ±10 mm and ±10° on 1 representative EAM.

As the agreement between voltage and PSI is thought to be affected by each modality's spatial resolution and noise, we sought to modulate spatial resolution and reduce noise by implementing spatial smoothing. This assigns to each point in a map the average value of its neighboring points within a given radius. Systematic variation of this radius (circular linear filters with radius equal to 2, 4, and 6 mm) allowed evaluation of the impact of spatial resolution/noise reduction on agreement between EAM voltage and PSI. Video 2 shows the effect of increasing spatial smoothing on representative voltage and PSI maps.

STATISTICAL ANALYSIS. Data distribution is reported as median, first to third quartile. Correlation was assessed using the Spearman's correlation coefficient (r). Assessment of binary classification of low-voltage zones characterized by V <0.5 mV or V <1.5 mV was performed using receiver-operating characteristic (ROC) curves. The area under the receiver-operating characteristic curve (AUC) as well as sensitivity and specificity obtained using the optimum PSI threshold (threshold corresponding to the point closest to 100 sensitivity and specificity) were estimated for each case. Sensitivity and specificity were then assessed using a fixed PSI threshold equal to the median value of case-specific PSI thresholds. EAM for which the prevalence of low-voltage zones was <3% were not considered. Reported results represent averaged values across CMR layers spanning from subendocardium (layer 10%) to mid-myocardium (layer 50%) included. Results for each layer are reported in the Supplemental Material.

RESULTS

CMR scans were performed without complication in all subjects, with no significant changes in device parameters (battery voltage or lead sensitivities, thresholds, or impedances) between pre- and post-CMR device interrogations. PSI scar maps were free from artefact in 3 of the 10 patients. In the 7 remaining patients, artefacts were most frequently located at the apical cap (n = 4) and on the anterior wall (n = 3) (Supplemental Figure S1). The proportion of LV surface affected by artefacts was 9.7% (1.4%-13.9%) across patients. The median interval between CMR and electrophysiological study was 2 days (5-23 days), with no relevant clinical events between procedures in any patient (Table 1).

Meshes of EAMs were derived from 611 electrode points (385-1,581 electrode points) and were composed of 7,859 vertices (6,880-14,952 vertices), of which 59% (48%-65%) were paired to CMR points (Table 2), with the remaining ones often belonging to nonventricular structures or the valve plane, or being proximal to CMR artefacts. Pooling data from all cases, the distance between CMR and EAM points was 3.36 mm (1.64-5.28 mm). Of all EAM points, 87% and 13% were collected using a Pentaray and a standard ablation catheter, respectively. In 3 cases, intracardiac electrograms were mainly collected with the ablation catheter. In 2 of these, all points in the EAM meshes had contact force >2*g*. In the remaining case, 27% of points in the EAM mesh had either undetermined force or force <2*g*.

On CMR, end diastolic and systolic volumes were 248 mL (197-290 mL) and 187 mL (141-227 mL), respectively. There was a good agreement between

FIGURE 1 **Comparison Between EAM and LGE-CMR (Example Subject #9)**

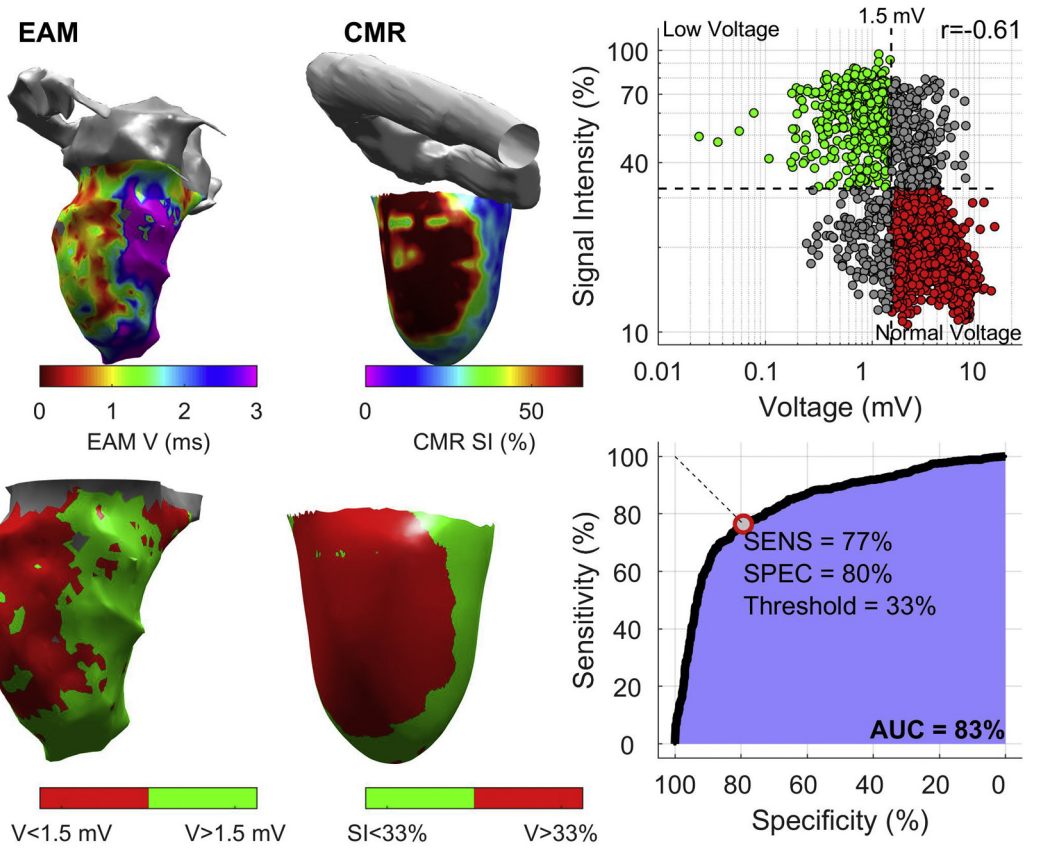

(Top) Voltage and CMR-intensity maps (30 transmurality) shown side-by-side. **(Bottom)** Low-voltage areas (V <1.5 mV) and areas with PSI >33% indicating abnormal tissue are shown on the **left and right**, respectively. Maps from **left to right** are shown in the same reference system. **Top right inset** shows correlation between voltage and PSI (on loglog scale), with **green** representing true positives and **red** representing true negative. Correlation coefficient was r = −0.61. **Bottom-right panel** shows receiver-operating characteristic curve with a **red circle** representing optimal threshold for identification of low-voltage zones. AUC = area under the receiver-operating characteristic curve; CMR = cardiovascular magnetic resonance; EAM = electroanatomic map; LGE = late gadolinium enhancement; PSI = pixel signal intensity; SENS = sensitivity; SPEC = specimen.

the area of the LV (excluding the valve plane) measured from EAM and CMR geometries, with correlation coefficient equal to r = 0.879 (Supplemental Figure S8). The LV area from EAM was 0.3% (−3.5% to 7.3%) larger than LV area from CMR.

CORRELATION BETWEEN EAM VOLTAGE AND PSI. Comparison between EAM and PSI maps for 2 representative patients, including point-by-point correlations and case-specific ROC curves, is shown in **Figure 1** and Supplemental Figure S2.

A significant negative correlation between bipolar voltage and PSI was registered in all patients across all cardiac sites, with a correlation coefficient equal to −0.57 (−0.68 to −0.42). PSI correlation with unipolar voltage was also significant, but lower, with correlation coefficient equal to −0.49 (−0.65 to −0.36). Correlation between endocardial bipolar voltage and PSI and between endocardial unipolar voltage and PSI was not significantly different across different transmural layers, from endocardial to epicardial PSI layers (Supplemental Figure S3).

AGREEMENT IN LVZ LOCALIZATION. Case by case ROC analyses showed good localization of low-voltage zones (**Table 2**), with median AUC for the localization of areas with V <1.5 mV of 0.82 (IQR: 0.76-0.83), sensitivity of 74% (IQR: 71%-77%), and specificity of 78% (IQR: 73%-83%) (results shown as median [IQR] of case-by-case ROC analysis). Localization of areas with V <0.5 mV was similar (**Table 2**). The correlation coefficient between the area of low-voltage zones from EAM and PSI maps was 0.87 for V <0.5 mV and 0.79 for V <1.5 mV (**Figure 2**). Agreement between CMR and

FIGURE 2 Correlation Between Scar Area on EAM and CMR-LGE

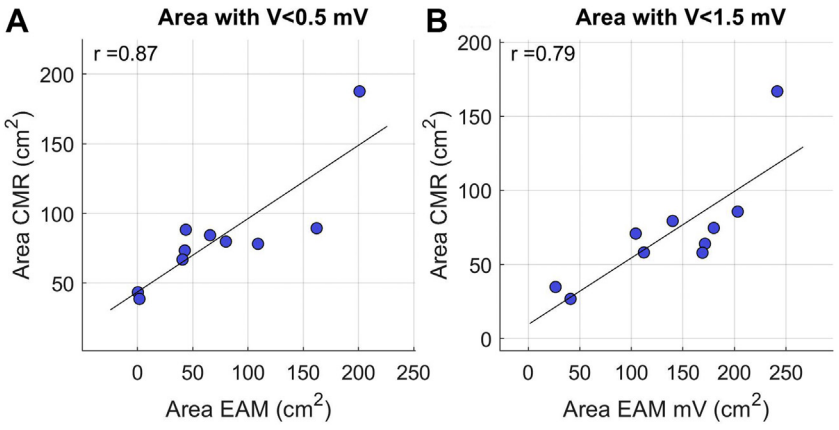

Linear fitting is reported with a **solid line** and correlation coefficient (r) is shown on the **top-left corner**. On EAM, low-voltage zones were defined with V <0.5 mV **(A)** and V <1.5 mV **(B)**. On CMR maps, areas representing low-voltage zones were identified with case-specific thresholds obtained through receiver-operating characteristic analysis (average of layers spanning from subendocardium, layer 10, to mid-myocardium, layer 50). Abbreviations as in **Figure 1**.

EAM for localization of LVZ was similar in cases where the majority of data was collected using an ablation catheter (n = 3) and where a Pentaray (n = 7) catheter was used (Supplemental Table S1).

These results were obtained using case-specific ROC-derived PSI thresholds. Similar results were obtained when using a fixed PSI threshold for all cases, taken as the median value of the case-specific PSI thresholds (ie, PSI >41% for V <1.5 mV and PSI >46% for V <0.5 mV) (**Table 2**). Sensitivity and specificity were 71% (65%-81%) and 76% (69%-86%) for V <1.5 mV, and 79% (62%-86%) 67% (67%-77%) for V <0.5 mV, respectively.

As expected, given that voltage maps were collected on the endocardium, low-voltage zones localization was more accurate using endocardial than epicardial PSI layers (Supplemental Figure S4). However, accuracy in low-voltage zones localization using PSI was not significantly different for the subendocardial compared to midmyocardial layer (Supplemental Figure S4).

Across all patients, mean PSI at ablation sites was 65% (63%-73%), and 93% (83%-100%) of ablation sites were located in areas of scar (ie, above PSI threshold) in PSI maps. The distribution of ablation sites mapped onto a coregistered PSI map, including electrograms recorded at a cardiac site where ablation terminated a subsequently induced VT, is shown for 1 case in **Figure 3**.

Choosing a different minimum distance required for pairing CMR and EAM points modified the number of paired sites without significantly affecting the results (Supplemental Figure S7). Finally, rescaling PSI values to their 5th and 95th percentile value instead of between minimum and maximum did not affect the results (Supplemental Table 2).

EFFECT OF COREGISTRATION MISALIGNMENTS. Results of the simulation study to assess low-voltage zones localization after algorithmically altering coregistration showed that misalignments can have a strong impact on the agreement between PSI and voltage, with both PSI-voltage correlation and discrimination of low-voltage zones decreasing for increasing shifts/rotations (**Figure 4A**). Nevertheless, intraoperator and interoperator coregistration variability had little impact on low-voltage zones localization (**Figure 4B**). The position of the aligned geometries after repeated coregistrations differed by few millimeters (median absolute shift along X, Y, and Z axes was equal to 2.6, 2.9, and 2.3 mm, respectively) and degrees (median absolute rotation about X, Y, and Z axes was equal to 4.7°, 3.1°, and 13.3°, respectively) (Supplemental Table 3). Pairwise correlation coefficients between AUC obtained using reference and additional coregistrations ranged between 0.83 and 0.88, whereas intraclass correlation coefficients measuring the agreement between AUC estimates across all configurations was equal to 0.86 and 0.88 for localization of V <1.5 mV and V <0.5 mV, respectively (Supplemental Figure S5).

EFFECT OF SPATIAL SMOOTHING. Spatial smoothing gradually improved agreement between voltage and PSI maps. Maximum smoothing (R = 6 mm) in both PSI and voltage resulted in an increase in median PSI-

FIGURE 3 VT Critical Sites on Electroanatomical Map and CMR-Pixel-Intensity Signal Intensity

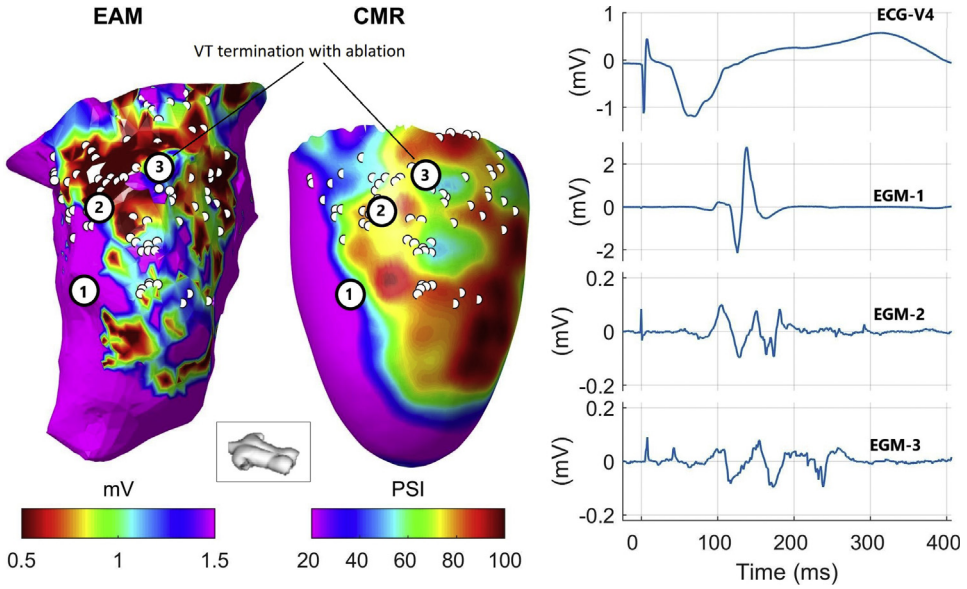

(Left) EAM collected while pacing from the RV apex and CMR PSI map (endocardial layer corresponding to 10% of wall thickness). **White dots** indicate ablation sites projected onto the 2 geometries. Electrograms (EGM) from sites labelled 1 (healthy tissue), 2 (dense scar), and 3 (VT exit site) are shown on the **right** as EGM-1, -2, and -3. Ablation proximal to site 3 terminated ventricular tachycardia induced after substrate mapping. Note that the y-scale is adjusted to the signal's amplitude. Abbreviations as in **Figure 1**.

voltage correlation coefficient of 13.7% ($P = 0.002$) (**Figure 4C**) and in median AUC of 5.8 ($P = 0.004$) (**Figure 4C**) with respect to nonsmoothed maps. Effect of spatial smoothing applied in isolation or in combination to PSI and voltage maps is described in detail in the Supplemental Material (Supplemental Figure S6).

DISCUSSION

The aim of this study was to assess performance and limitations of low-voltage zones (LVZ) localization by optimized LGE-CMR scar imaging in patients with CIEDs and coregistration algorithms for the delineation of scar in patients with CIEDs. We applied state of the art CMR imaging and electro-anatomical mapping to quantify spatial correlation between EAM voltage and PSI across all cardiac sites, focusing on the impact of coregistration and spatial resolution.

The main findings are as follows (**Central Illustration**): 1) PSI showed a significant inverse correlation with EAM voltage (r = −0.57; IQR: −0.68 to −0.42) and allowed localization of low-voltage zones with median sensitivity and specificity of 74% and 78%; 2) small variations in EAM-CMR anatomical coregistration can worsen the localization of low-voltage zones, but the use of the ascending and descending aorta to guide coregistration ensures high intraoperator and interoperator reproducibility.

With increasing numbers of patients with CIEDs considered for VT ablation caused by recurrent arrhythmias and appropriate shocks, techniques are required to improve procedural success rates while reducing radiation dose and procedural times. LGE-CMR can aid scar localization and preprocedural planning (2-7,16); however, CMR in patients with CIEDs has generally been avoided because of concerns related to risk and poor image quality from device-related artefact. Few studies had previously investigated EAM and CMR in patients with CIEDs. These had focused on scar size (13), feasibility (17), and correlation between critical sites for re-entry initiation (8), but localization of low-voltage zones by CMR, which is crucial for VT catheter ablation, is still undetermined. This study provides the first assessment of the agreement between voltage and PSI maps in patients with CIEDs. Importantly, it provides quantitative assessment of the impact of coregistration misalignments, which has significant implications particularly in the context of a purely anatomic scar mapping strategy to identify corridors that support re-entry (8,9). Indeed, a recent study has shown

FIGURE 4 EAM-CMR Agreement

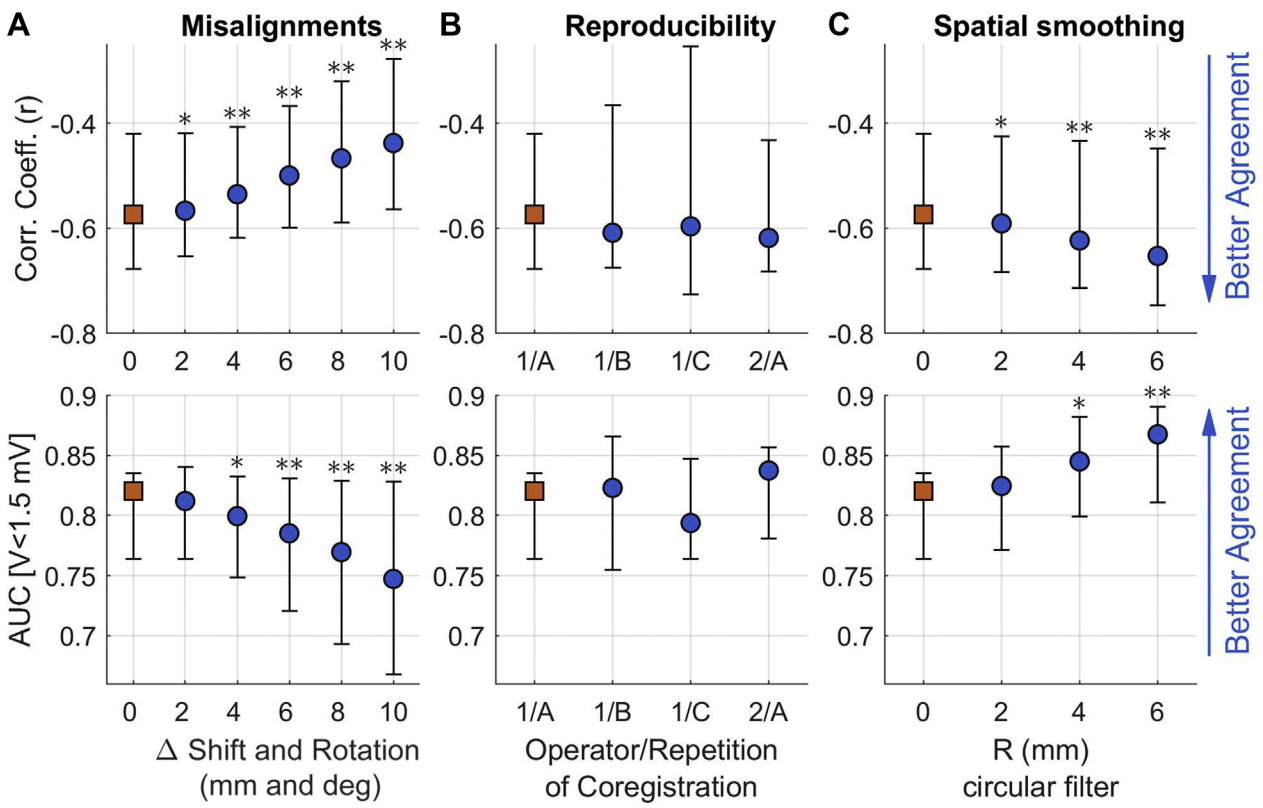

Effect of misalignment in coregistration **(A)**, interoperator and intraoperator variability of coregistration **(B)**, and spatial smoothing of voltage and PSI maps **(C)** on EAM-CMR agreement. **(A)** Expert-based coregistration of each case was algorithmically modified by simultaneously shifting (Δmm) and rotating (Δdeg) the voltage map along and across the 3 orthogonal axes (64 iterations per Δ and patient). **(B)** EAM and voltage maps were coregistered by a first operator 3 times (1A, 1B, and 1C) and by a second operator (2A). **(C)** Increasing degree of spatial smoothing of voltage and PSI maps using a circular filter of radius equal to 2, 4, and 6 mm. **Markers and whiskers** represent median value and interquartile range. r = Spearman's correlation coefficient between PSI and voltage across cardiac sites. AUC = area under the receiver-operating characteristic curve for localization of zones with V <1.5 mV. *$P < 0.05$; **$P < 0.005$ (Wilcoxon signed rank test) with respect to reference values (**red squares**, corresponding to Δ = 0 in **A**; 1A in **B**; R = 0 in **C**). Abbreviations as in **Figure 1**.

that CMR-guided catheter ablation based on localization of critical sites of VT through advance image processing of PSI maps can reduce procedural time and improve outcomes of VT catheter ablation (9). Another potential application for CMR may be in combination with other noninvasive modalities to identify ablation target for stereotactic body radiotherapy (18,19). For instance, ECG imaging could be used for identification of VT sites of origin and delineation of the functional electrophysiological substrate related to activation and repolarization abnormalities (14,15,20), whereas CMR could be used for scar delineation and identification of corridors supporting the VT circuit.

IMPACT OF EAM-CMR COREGISTRATION. Coregistration usually involves minimization of the distance between landmark points, followed by manual adjustment by expert operators. This can introduce bias, particularly if only LV models are used for alignment. We assessed the impact of small random alterations in the coregistration by algorithmically applying rotations and shifts to the EAM after coregistration. We found that these had an impact and that in some cases even small rotations and shifts considerably reduced the agreement between voltage and PSI maps. Despite this, we found that intraoperator and interoperator coregistration variability was low, and reproducibility of low-voltage zones localization was high (intraclass correlation of AUC = 0.86). This is the first study to assess the reproducibility of coregistration, which in this study was optimized by the utilization of the full 3D geometry of the ascending, arch, and descending aorta.

CENTRAL ILLUSTRATION **Low-Voltage Zone Localization by Cardiac MRI in Patients With Implantable Devices**

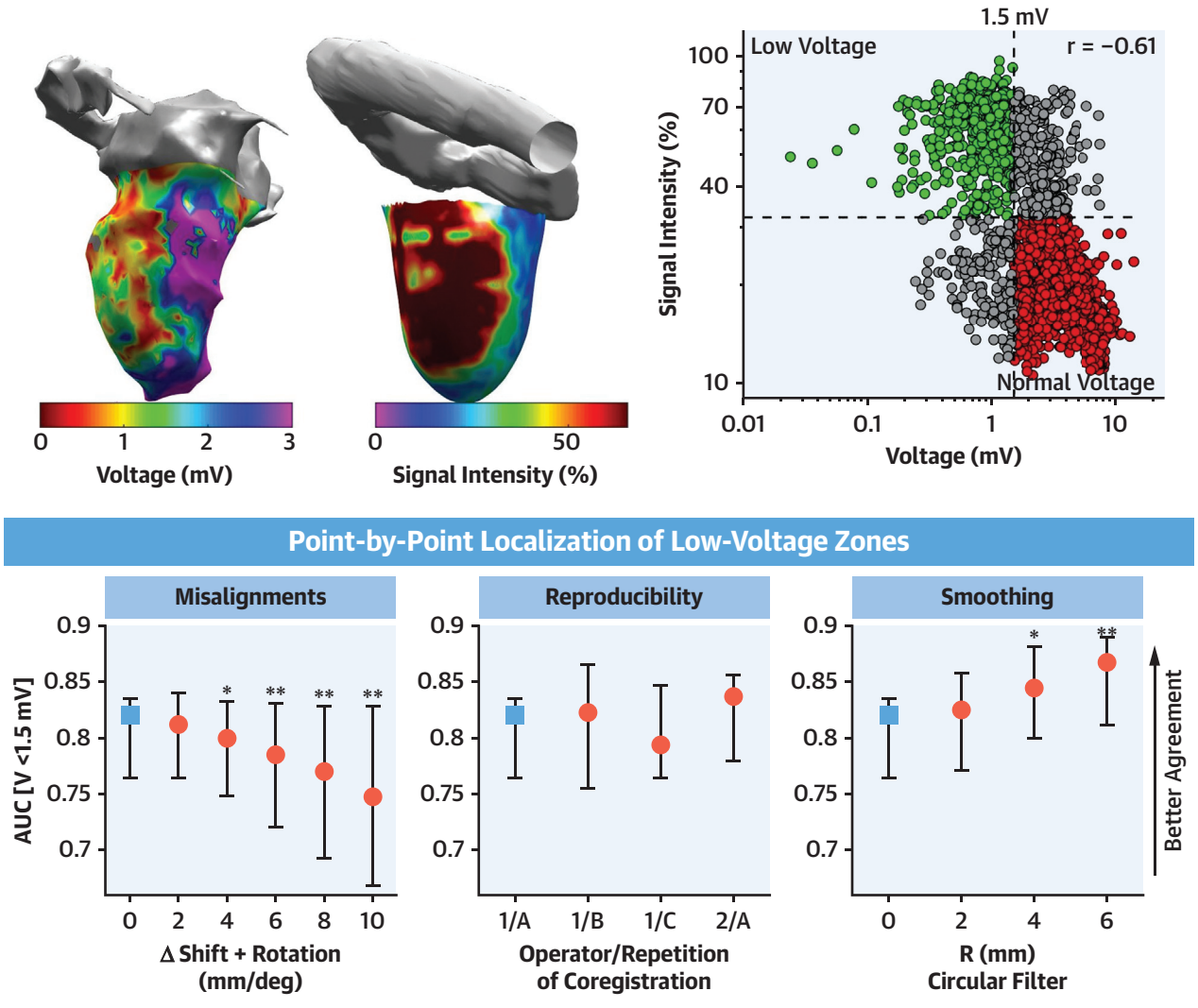

Orini, M. et al. J Am Coll Cardiol EP. 2022;8(2):225–235.

AUC = area under the receiver-operating characteristic curve; CIED = cardiac implantable electronic device; MRI = magnetic resonance imaging.

The use of the full aortic geometry to coregister CMR and electroanatomical data was proposed in one of the seminal studies on EAM-CMR integration (21) but has not been adopted as standard clinical practice. Previous studies have used other anatomical landmarks for coregistration, including the position of the mitral annulus, proximal aorta, pulmonary artery, RV, or the ostium of the left main coronary artery (4,9), and 1 study has analyzed the effects of rotation (but not shifts) on coregistration accuracy (22).

METHODOLOGICAL CONSIDERATIONS. LGE-CMR correlates well histologically with various models of myocardial fibrosis (23), but quantitative evaluation of LGE is challenging, with signal thresholding affecting the projected infarct size. Despite good correlation between EAM voltage and PSI using fixed thresholds based on the median values across the cohort, the optimal PSI threshold varied considerably across cases, and there was a narrow gap between optimum thresholds for localization of low-voltage

zones with V <1.5 mV and V <0.5 mV. This highlights the challenge of delineating scar border-zones (0.5-1.5 mV), which beyond the limitations of spatial resolution inherent to each modality may be related to the effect of wall thickness (24), catheter configuration (25), variable CMR contrast kinetics or residual hypersensitivity and signal void related to the presence of the ICD.

In primary analysis, we have reported averaged values across CMR layers spanning from subendocardium (layer 10%) to midmyocardium (layer 50%). Layer-by-layer analysis has shown that localization of endocardial low-voltage zones was more accurate when using endocardial layers compared with epicardial layers (Supplemental Figure S4). However, accuracy in low-voltage zones localization was not significantly different in the subendocardial PSI layers compared with midmyocardial layers. There are several possible explanations for this, which relate to the limitations of the respective techniques. Although midmyocardial scar may be less apparent on endocardial EAM, there are also challenges in segmenting the true endocardium with CMR and accurately demonstrating the blood-myocardial boundary. The proximity of the 10% layer to the blood pool may occasionally result in partial volume effects within the endocardial voxel, which might introduce artefact in the reconstructed 3D model. Despite attempts to limit this by using thin 2D slices (4 mm), in some cases this cannot be corrected. This limitation is further accentuated in cases of severe ischemic cardiomyopathy in view of the reduced wall thickness of infarcted myocardium.

Correlation between endocardial unipolar voltage and PSI was similar across all PSI layers, including deeper midmyocardial and subepicardial layer (Supplemental Figure S3). Although endocardial unipolar voltage has been shown to enable localization of epicardial scar, evidence is stronger for nonischemic cardiomyopathy and in absence of endocardial scar (26). Furthermore, theoretical (27) and experimental (28) studies have demonstrated that the amplitude of the unipolar electrogram is mainly determined by remote activity (and in particular by the sequence of electrical depolarization), and therefore, it is not an ideal parameter for localization of scar.

In this study, we used spatial smoothing to reduce noise in both voltage and PSI maps. Spatial smoothing improved agreement between voltage and PSI maps with moderate but significant increase in voltage-PSI correlation and low-voltage zone discrimination. However, because smoothing reduces spatial resolution, its use may be limited to the localization of large areas of scar as opposed to the fine details of the scar architecture.

STUDY LIMITATIONS. Our study is limited by the small sample size. However, patients had high-density EAM and complete geometry of the aorta, which is crucial to ensure detailed delineation of the substrate and optimal coregistration. EAM was used as a reference for the identification of abnormal tissue, and although Pentaray was used to collect most points, an ablation catheter was occasionally used. Bipolar voltage can be affected by wave front directionality and catheter configuration (25). Although higher spatial resolution LGE imaging can be obtained using 3D MRI ($1.9 \times 1.9 \times 1.9$ μL), 3D wideband LGE imaging is generally unfeasible in patients with frequent ventricular arrhythmias awaiting ablation. Finally, this study was limited to endocardial maps and did not focus on the utility of integrating CMR with EAM data during catheter ablations (6-8). This, however, should be the focus of further investigation.

CONCLUSIONS

In patients with CIEDs, the use of novel wideband CMR LGE sequences and strategies to optimize coregistration can localize areas of scar with good accuracy. To fully establish the role of CMR in assisting VT ablation, effort should be focused on standardizing coregistration, improving data acquisition and reducing noise in both modalities.

FUNDING SUPPORT AND AUTHOR DISCLOSURES

Drs Orini, Moon, Lambiase, and Manisty are directly and indirectly supported by the University College London Hospitals and Barts Hospital NIHR Biomedical Research Centres. Drs Seraphim and Bhuva are supported by doctoral research fellowships from the British Heart Foundation (FS/16/46/32187 and FS/18/83/34025). Dr Lambiase has received research grants from Boston Scientific, Medtronic, and Abbott; and has received speaker fees from Medtronic. All other authors have reported that they have no relationships relevant to the contents of this paper to disclose.

ADDRESS FOR CORRESPONDENCE: Prof Pier D. Lambiase, Institute of Cardiovascular Science, 5 University Street, London WC1E 6JF, United Kingdom. E-mail: p.lambiase@ucl.ac.uk. OR Dr Charlotte H. Manisty, Department of Cardiac Imaging, Barts Heart Centre, West Smithfield, London EC1A 7BE, United Kingdom. E-mail: c.manisty@ucl.ac.uk.

PERSPECTIVES

COMPETENCY IN MEDICAL KNOWLEDGE: This study shows that optimized CMR enables noninvasive localization of scar in patients with CIEDs and it highlights the importance of using the thoracic aorta as a landmark for accurate coregistration with EAMs.

TRANSLATIONAL OUTLOOK: Optimized CMR sequences and accurate coregistration of CMR scar maps with electroanatomical geometries could improve VT ablation.

REFERENCES

1. Graham AJ, Orini M, Lambiase PD. Limitations and challenges in mapping ventricular tachycardia: new technologies and future directions. *Arrhythmia Electrophysiol Rev*. 2017;6(3):118–124.

2. Ashikaga H, Sasano T, Dong J, et al. Magnetic resonance-based anatomical analysis of scar-related ventricular tachycardia: Implications for catheter ablation. *Circ Res*. 2007;101(9):939–947.

3. Codreanu A, Odille F, Aliot E, et al. Electro-anatomic characterization of post-infarct scars: comparison with 3-dimensional myocardial scar reconstruction based on magnetic resonance imaging. *J Am Coll Cardiol*. 2008;52(10):839–842.

4. Wijnmaalen AP, Van Der Geest RJ, Van Huls Van Taxis CFB, et al. Head-to-head comparison of contrast-enhanced magnetic resonance imaging and electroanatomical voltage mapping to assess post-infarct scar characteristics in patients with ventricular tachycardias: Real-time image integration and reversed registration. *Eur Heart J*. 2011;32(1):104–114.

5. Sramko M, Hoogendoorn JC, Glashan CA, Zeppenfeld K. Advancement in cardiac imaging for treatment of ventricular arrhythmias in structural heart disease. *Europace*. 2019;21(3):383–403.

6. Andreu D, Berruezo A, Ortiz-Pérez JT, et al. Integration of 3D electroanatomic maps and magnetic resonance scar characterization into the navigation system to guide ventricular tachycardia ablation. *Circ Arrhythmia Electrophysiol*. 2011;4(5):674–683.

7. Andreu D, Penela D, Acosta J, et al. Cardiac magnetic resonance–aided scar dechanneling: influence on acute and long-term outcomes. *Heart Rhythm*. 2017;14(8):1121–1128.

8. Roca-Luque I, Van Breukelen A, Alarcon F, et al. Ventricular scar channel entrances identified by new wideband cardiac magnetic resonance sequence to guide ventricular tachycardia ablation in patients with cardiac defibrillators. *Europace*. 2020;22(4):598–606.

9. Soto-Iglesias D, Penela D, Jáuregui B, et al. Cardiac magnetic resonance-guided ventricular tachycardia substrate ablation. *J Am Coll Cardiol EP*. 2020;6(4):436–447.

10. Bhuva AN, Kellman P, Graham A, et al. Clinical impact of cardiovascular magnetic resonance with optimized myocardial scar detection in patients with cardiac implantable devices. *Int J Cardiol*. 2019;279:72–78.

11. Seewöster T, Löbe S, Hilbert S, et al. Cardiovascular magnetic resonance imaging in patients with cardiac implantable electronic devices: best practice and real-world experience. *Europace*. 2019;21(8):1220–1228.

12. Dickfeld T, Tian J, Ahmad G, et al. MRI-guided ventricular tachycardia ablation integration of late gadolinium-enhanced 3D scar in patients with implantable cardioverter- defibrillators. *Circ Arrhythmia Electrophysiol*. 2011;4(2):172–184.

13. Stevens SM, Tung R, Rashid S, et al. Device artifact reduction for magnetic resonance imaging of patients with implantable cardioverter-defibrillators and ventricular tachycardia: Late gadolinium enhancement correlation with electroanatomic mapping. *Heart Rhythm*. 2014;11(2):289–298.

14. Graham AJ, Orini M, Zacur E, et al. Simultaneous comparison of electrocardiographic imaging and epicardial contact mapping in structural heart disease. *Circ Arrhythmia Electrophysiol*. 2019;12(4):e007120.

15. Graham AJ, Orini M, Zacur E, et al. Evaluation of ECG imaging to map haemodynamically stable and unstable ventricular arrhythmias. *Circ Arrhythmia Electrophysiol*. 2020;13(2):e007377.

16. Desjardins B, Crawford T, Good E, et al. Infarct architecture and characteristics on delayed enhanced magnetic resonance imaging and electroanatomic mapping in patients with post-infarction ventricular arrhythmia. *Heart Rhythm*. 2009;6(5):644–651.

17. Singh A, Kawaji K, Goyal N, et al. Feasibility of cardiac magnetic resonance wideband protocol in patients with implantable cardioverter defibrillators and its utility for defining scar. *Am J Cardiol*. 2019;123(8):1329–1335.

18. Robinson CG, Samson PP, Moore KMS, et al. Phase I/II trial of electrophysiology-guided noninvasive cardiac radioablation for ventricular tachycardia. *Circulation*. 2019;139(3):313–321.

19. Cuculich PS, Schill MR, Kashani R, et al. Noninvasive cardiac radiation for ablation of ventricular tachycardia. *N Engl J Med*. 2017;377(24):2325–2336.

20. Wang Y, Cuculich PS, Zhang J, et al. Noninvasive electroanatomic mapping of human ventricular arrhythmias with electrocardiographic imaging. *Sci Transl Med*. 2011;3(98):98ra84.

21. Reddy VY, Malchano ZJ, Holmvang G, et al. Integration of magnetic resonance imaging with three-dimensional electroanatomic mapping to guide left ventricular catheter manipulation: feasibility in a porcine model of healed myocardial infarction. *J Am Coll Cardiol*. 2004;44(11):2202–2213.

22. Tao Q, Milles J, Van Huls Van Taxis C, et al. Toward magnetic resonance-guided electroanatomical voltage mapping for catheter ablation of scar-related ventricular tachycardia: A comparison of registration methods. *J Cardiovasc Electrophysiol*. 2012;23(1):74–80.

23. Iles LM, Ellims AH, Llewellyn H, et al. Histological validation of cardiac magnetic resonance analysis of regional and diffuse interstitial myocardial fibrosis. *Eur Heart J Cardiovasc Imaging*. 2015;16(1):14–22.

24. Glashan CA, Androulakis AFA, Tao Q, et al. Whole human heart histology to validate electroanatomical voltage mapping in patients with non-ischaemic cardiomyopathy and ventricular tachycardia. *Eur Heart J*. 2018;39(31):2867–2875.

25. Takigawa M, Relan J, Kitamura T, et al. Impact of spacing and orientation on the scar threshold with a high-density grid catheter. *Circ Arrhythmia Electrophysiol*. 2019;12(9):e007158.

26. Hutchinson MD, Gerstenfeld EP, Desjardins B, et al. Endocardial unipolar voltage mapping to detect epicardial ventricular tachycardia substrate in patients with nonischemic left ventricular cardiomyopathy. *Circ Arrhythmia Electrophysiol*. 2011;4(1):49–55.

27. Potse M, Vinet A, Opthof T, Coronel R. Validation of a simple model for the morphology of the T wave in unipolar electrograms. *Am J Physiol Heart Circ Physiol*. 2009;297(2):H792–H801.

28. Orini M, Taggart P, Lambiase PD. In vivo human sock-mapping validation of a simple model that explains unipolar electrogram morphology in relation to conduction-repolarization dynamics. *J Cardiovasc Electrophysiol*. 2018;29(7):990–997.

KEY WORDS ablations, cardiac mapping, cardiovascular MRI, scar, ventricular tachycardia

APPENDIX For supplemental figures, tables, and videos, please see the online version of this paper.